Springtime Soil Moisture Teleconnections Drive Summertime Warming in the Western United States

Lily N. Zhang,[a] David S. Battisti,[a] Lucas R. Vargas Zeppetello,[b] Marysa M. Laguë[c]

[a] *Department of Atmospheric and Climate Science, University of Washington, Seattle, WA*

[b] *Department of Environmental Science, Policy, and Management, University of California, Berkeley, Berkeley, CA*

[c] *Department of Geography, University of British Columbia, Vancouver, BC, Canada*

Corresponding author: Lily N. Zhang, lnzhang@uw.edu

Manuscript under review at the Journal of Climate.

ABSTRACT

A prior study observed that regional variations in springtime soil moisture over the American Southwest are associated with distal summertime temperature and precipitation anomalies across the Western United States. Here, we perform an ensemble of soil moisture depletion experiments within the Community Earth System Model (CESM2) and show that a reduction in March surface soil moisture over the Southwest US causes positive May-June temperature anomalies throughout the Western US and precipitation anomalies in the Northwest that are consistent with observations. In our experiments, daytime diabatic heating over anomalously dry land surfaces in early spring excites circulation anomalies that evolve into a hemispheric-scale pattern similar to that observed following anomalously dry springtime in the Southwest US. We show that the subsequent late spring and early summer circulation anomalies are associated with large-scale reductions in atmospheric moisture and cloudiness that contribute to the near-surface warming. Our results suggest that land-atmosphere coupling provides a pathway for soil moisture variations to become a source of predictability on seasonal time scales in the Western US.

SIGNIFICANCE STATEMENT

Observations show that warmer-than-average summertime temperatures in the Western US are often preceded by drier-than-average spring soils in the Southwest US. We perform experiments within a global climate model and demonstrate the causal mechanism for this phenomenon: early spring soil moisture deficits in the Southwest US cause anomalously warm summers throughout the Western US through their effect on the large-scale atmospheric circulation.

1. Introduction

Temporally lagged correlations between climate state variables are an important indicator of predictability in the climate system. When these relationships extend across large spatial scales, they give rise to so-called “teleconnections” that are typically associated with prominent models of climate variability (Ångström 1935). Most notably, variations in sea surface temperature (SST) associated with the El Niño Southern Oscillation (ENSO) are known to influence precipitation at distal locations through atmospheric teleconnection pathways between the tropical Central Pacific and other parts of the world (Walker and Bliss 1932; Ropelewski and Halpert 1987; Trenberth et al. 1998). Less well-studied are the

teleconnection-like behaviors observed in other slow-varying components of the coupled climate system, such as land and sea ice (Teng et al. 2019; Xue et al. 2022; Liu et al. 2023).

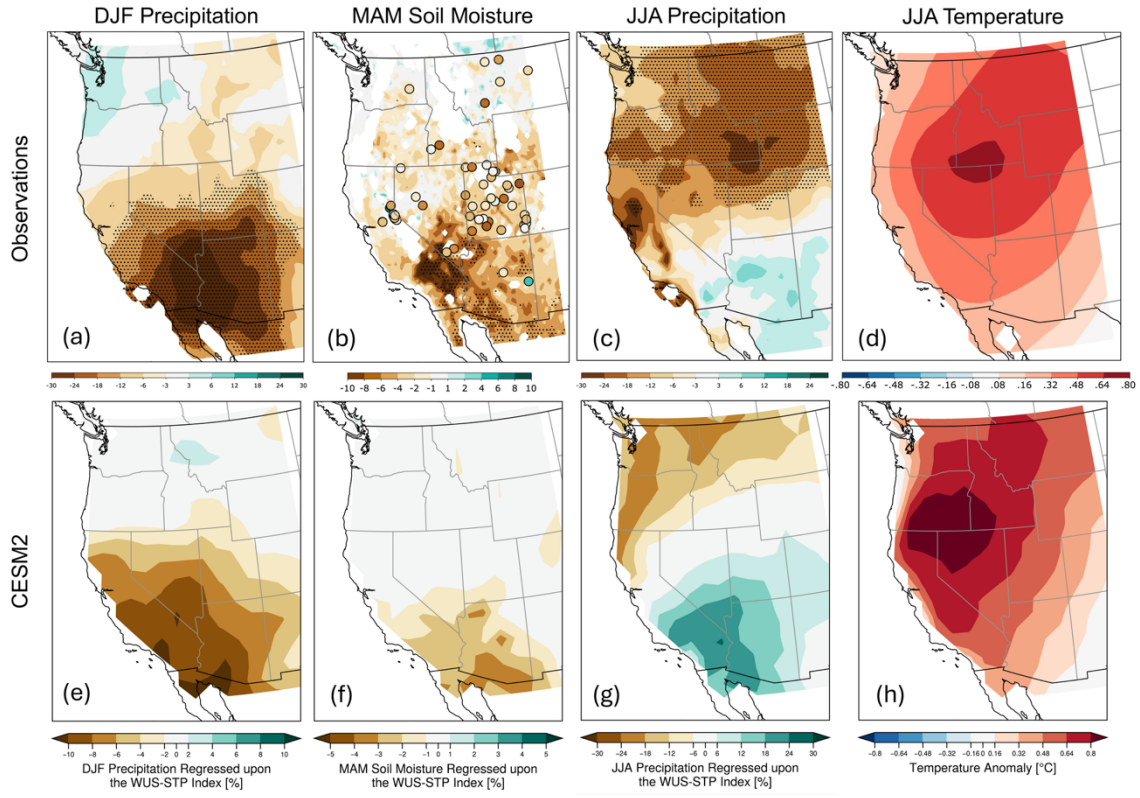

Fig. 1. EOF1 of high pass-filtered JJA average temperatures across the Western US domain (105-130 W, 30-50 N) in observations (panel d) and in the CESM2 historical simulation (panel h). Preceding (a) DJF precipitation (b) MAM soil moisture and contemporaneous (c) JJA precipitation anomalies regressed upon the WUS index (PC1 of JJA temperature) in observations. Panels (e-g) are as in panels (a-c), but for the WUS index from CESM2. The WUS-STP pattern captures 54% of summertime temperature variability over the domain in both CESM2 and observations. Variations in soil moisture and precipitation are expressed as percentages relative to the climatological seasonal mean. Figure reproduced from Vargas Zeppetello et al. (2024). See methods for a description of data sources.

A recent study by Vargas Zeppetello et al. (2024) found that interannual summertime temperature variations associated with the leading pattern of Western US summertime temperature variability are anticorrelated with antecedent springtime soil moisture variations. Across CMIP models and in observations, springtime soil moisture deficits in the Southwest US are linked to summertime precipitation deficits and anomalously high temperature across much of the Western US (Fig. 1). Unlike many patterns of climate variability, the Western US summertime temperature pattern (WUS-STP) displays weak and mostly statistically insignificant relationships with SST variability in summer and in the preceding seasons (Vargas Zeppetello et al. 2024)—suggesting that distal soil moisture anomalies influence climate in subsequent seasons in a teleconnection-like manner through land-atmosphere interactions alone.

Soil moisture anomalies modulate the partitioning of surface latent and sensible heat fluxes and thus act as a local diabatic heating source over dry surfaces (Seneviratne et al. 2010). Locally, feedbacks between soil moisture, near-surface temperature, and precipitation have been shown to contribute to the persistence of extreme events such as heatwaves and drought (Schär et al. 1999; Lorenz et al. 2010; Zhou et al. 2019; Vargas Zeppetello et al. 2022). The time scales of these local interactions can extend over several months in some regions, making soil moisture a valuable source of seasonal predictability (Delworth and Manabe 1989; Fennessy and Shukla 1999; Dirmeyer 2000; Wu and Dickinson 2004; Koster et al. 2010, 2011; Guo et al. 2011; Paolino et al. 2012). Of particular relevance to our study is the work by Fischer et al. (2007) who used a regional climate model forced by real-world lateral boundary conditions to investigate the role of soil moisture-atmosphere interactions during the 2003 European summer heat wave. Their sensitivity experiments showed that preceding spring soil moisture deficits in France amplified the summertime temperature anomalies through their effect on the local surface energy budget. There is strong evidence to suggest that the contiguous United States (CONUS) is another such region where soil moisture variations can exhibit strong "memory" characteristics on seasonal time scales (Liu et al. 2014; McColl et al. 2017; Rahmati et al. 2024). Rind (1982) used an atmosphere general circulation (AGCM) to demonstrate that reducing June soil moisture within the interior of the United States led to significantly higher near-surface temperature throughout CONUS during the summer. Namias (1991) hypothesized that antecedent soil moisture variations in early spring were a key indicator of anomalously low rainfall over the northern Great Plains in the summer of 1988. A later study by Pal and Eltahir (2001) similarly concluded that feedbacks between antecedent soil moisture conditions and convective rainfall played a significant role in maintaining the persistence of the 1988 drought in a series of regional model experiments. More generally, Wu et al. (2007) examined co-variability between spring soil moisture and summer precipitation and found statistically significant correlations over CONUS in a 50-year AGCM simulation. These early modeling studies all point to a link between spring soil moisture variations and summertime climate over the United States that is consistent with observations of the Western US summertime temperature pattern (Vargas Zeppetello et al. 2024).

Although the ability for antecedent soil moisture variations to influence climate beyond a single season has been established in models and observations, the spatial scales of these interactions are not as well understood. A few studies have explored the possibility for soil

moisture anomalies to have non-local impacts through feedbacks that modify the atmospheric circulation, particularly in monsoonal regions (Shukla and Mintz 1982; Small 2001; Douville 2002; Rai et al. 2015; Berg et al. 2017; Ullah et al. 2021). A recent study by Teng et al. (2019) demonstrated that prescribing soil moisture deficits over select CONUS domains led to circumglobal circulation changes that produced a robust, non-local climate response. In their AGCM experiments, diabatic heating anomalies generated by a prescribed deficit in summertime soil moisture excited stationary wave anomalies that resembled waveguide teleconnection patterns (Branstator 1990, 2002). On average, these non-local effects manifest as a hemispheric scale stationary wave train in the midlatitudes, including an anomalous high over the Pacific Northwest that matches the stationary wave response in similar experiments performed by Koster et al. (2016). With the aid of a stationary wave model, Koster et al. (2016) further confirmed that the diabatic heating anomalies attributed to rainfall deficits over CONUS land surfaces replicated the stationary wave response in the AGCM. It is notable that the contemporaneous temperature anomalies associated with the summertime wave train identified by Koster et al. (2016) and Teng et al. (2019) resemble the pattern of summertime temperature variability and associated fluctuations in geopotential height observed by Vargas Zeppetello et al. (2024).

In this study, we perform an ensemble of soil moisture depletion experiments to understand the physical processes behind the Vargas Zeppetello et al. (2024) finding that springtime soil moisture anomalies in the Southwest US cause non-local summertime temperature and precipitation anomalies throughout the Western US via soil moisture induced atmospheric teleconnections.

2. Methods

a. CESM2 soil moisture depletion experiments

We utilize the Community Earth System Model (CESM2; Danabasoglu et al. 2020) in an atmosphere/land-only configuration with prescribed phenology and pre-industrial forcings to isolate the physical mechanisms without the confounding influences of SST coupling and anthropogenic warming. The land and atmospheric components of CESM2 are the Community Land Model Version 5 (CLM5; Lawrence et al. 2019) and the Community Atmosphere Model Version 6 (CAM6), respectively. In place of a coupled ocean model, the CAM6 atmosphere in our experiments is forced by prescribed monthly mean SST sea ice

climatologies taken from the fully coupled CESM2 pre-industrial (PI) control run; simulations use PI (1850) CO2 levels of 285 ppm. We run this configuration, hereafter referred to as "CAM6-PI," at 0.9º x 1.25º resolution to obtain monthly output of relevant climate variables.

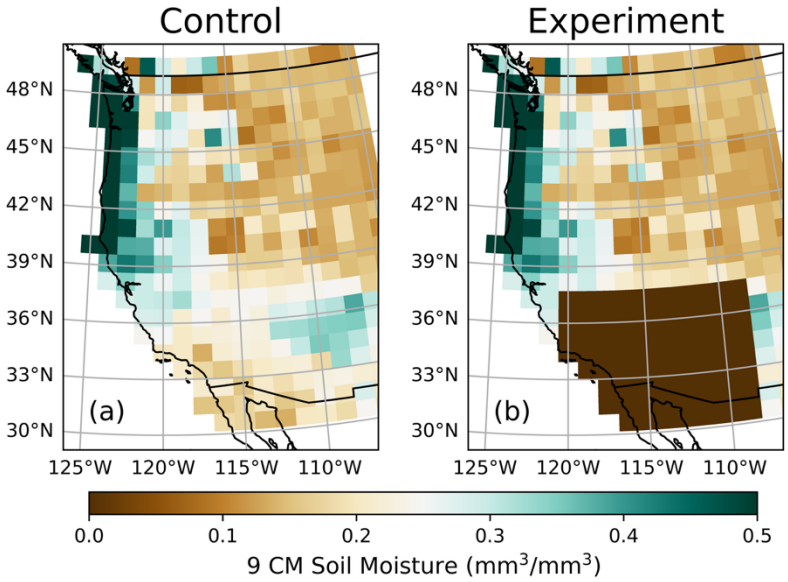

Fig. 2. Depth-weighted volumetric soil moisture content of the top three model layers (~9 cm) in the CLM restart files for March 1 of (left) an example control run year and (right) a Southwest US depletion experiment run in the same year.

Using CAM6-PI as a starting point, we instantaneously deplete soil moisture over a specified domain by modifying the soil liquid water field within the CLM restart files. In our experiments, we set the soil liquid water content of the top three model layers (~9 cm) to zero on March 1st of each simulation year for all land grids in the Southwest US, between 108-120ºW and 30-38ºN (Fig. 2). We chose to only modify the initialization of the land surface, rather than prescribe soil moisture deficit over a longer period (as was done in the Koster et al. (2016) and Teng et al. (2019)) to represent the observed effects of anomalously low wintertime precipitation on spring soil moisture in the Southwest US (Fig. 1a). When directly compared to a control run advanced with the same restart files (i.e., all else being equal), our experiment isolates the impact of anomalously dry land surfaces in the Southwest US on global climate over the timescales we are interested in—from the start of spring until summer.

The weak relationships between summertime temperature and spring soil moisture in CESM2 (c.f. Fig. 1b, 1f) motivated our use of what we thought would be a strong, idealized forcing at the start of the experiment to achieve the desired summertime response. However,

following this initial shock, soil moisture recovers fairly rapidly (Supplementary Figure S1). However, Furthermore, Vargas Zeppetello et al. (2024) showed seasonal mean surface soil moisture variations are coherent with soil moisture variations at depths up to 50 cm which suggests soil moisture anomalies at deeper layers are also important for land-atmosphere coupling. Integrating the soil moisture anomalies over the top 58 cm of the model, we find our soil moisture depletion amounts to a modest March average soil moisture deficit of 1.2σ anomaly relative to the model's typical year-to-year variations in March 58 cm soil moisture over the Southwest US. This year-to-year variability is represented well by the model (σ_{model} = 0.018 mm^3/mm^3, σ_{obs} = 0.016 mm^3/mm^3). The propagation of anomalies into deeper layers is evidence of vertical soil water transport in our experiments, which is governed by the one-dimensional Richards equation in CLM with parameters from observational estimates (Dingman 2002; Lawrence and Slater 2008).

To remove the influence of internal variability on our results, we examine an ensemble of soil moisture depletion experiments, each with a unique initial state. We create the ensemble by duplicating the restart files from a 108-year CAM6-PI control run. Then, in each March 1st restart file, we deplete the soil moisture in the Southwest domain (as above) and run the model for six months to the end of August, resulting in 108 soil depletion experiments. Each year of the experiment is initialized with the corresponding CAM6-PI year restart file, such that there is no signal of the current experiment year in the subsequent experiment year. All the results we present show evolution of the ensemble-mean difference between the control run and experiment, averaged across all 108 simulations, to yield the forced response to the soil moisture depletion under a variety of initial conditions. In general, the statistical significance of an anomaly is proportional to its magnitude (indicated by color) and darkly colored regions are statistically significant at $p < 0.10$.

b. Observational data sources

To compare the results of our modeling experiment with observation-based data, we obtain monthly mean 2-m temperature and 500 mb geopotential height from ERA5 (Hersbach et al., Accessed on 17-07-2025). We analyze these atmospheric variables alongside monthly averaged soil moisture values from 1992-2023, which are computed from daily satellite measurements from version 7 of the European Space Agency's Climate Change Initiative (CCI; Dorigo et al. 2017).

Figure 1, which was reproduced from Vargas Zeppetello et al. (2024), uses ESA CCI soil moisture from 2001-2020 and in-situ soil moisture from the International Soil Moisture Network (ISMN; Dorigo et al. 2021, shown in circles), station-based precipitation data from CRU TS (1981-2020; Harris et al. 2020), and temperature reconstructions from Berkeley Earth (1850-2021; Muller et al. 2014).

3. Near-surface temperature response

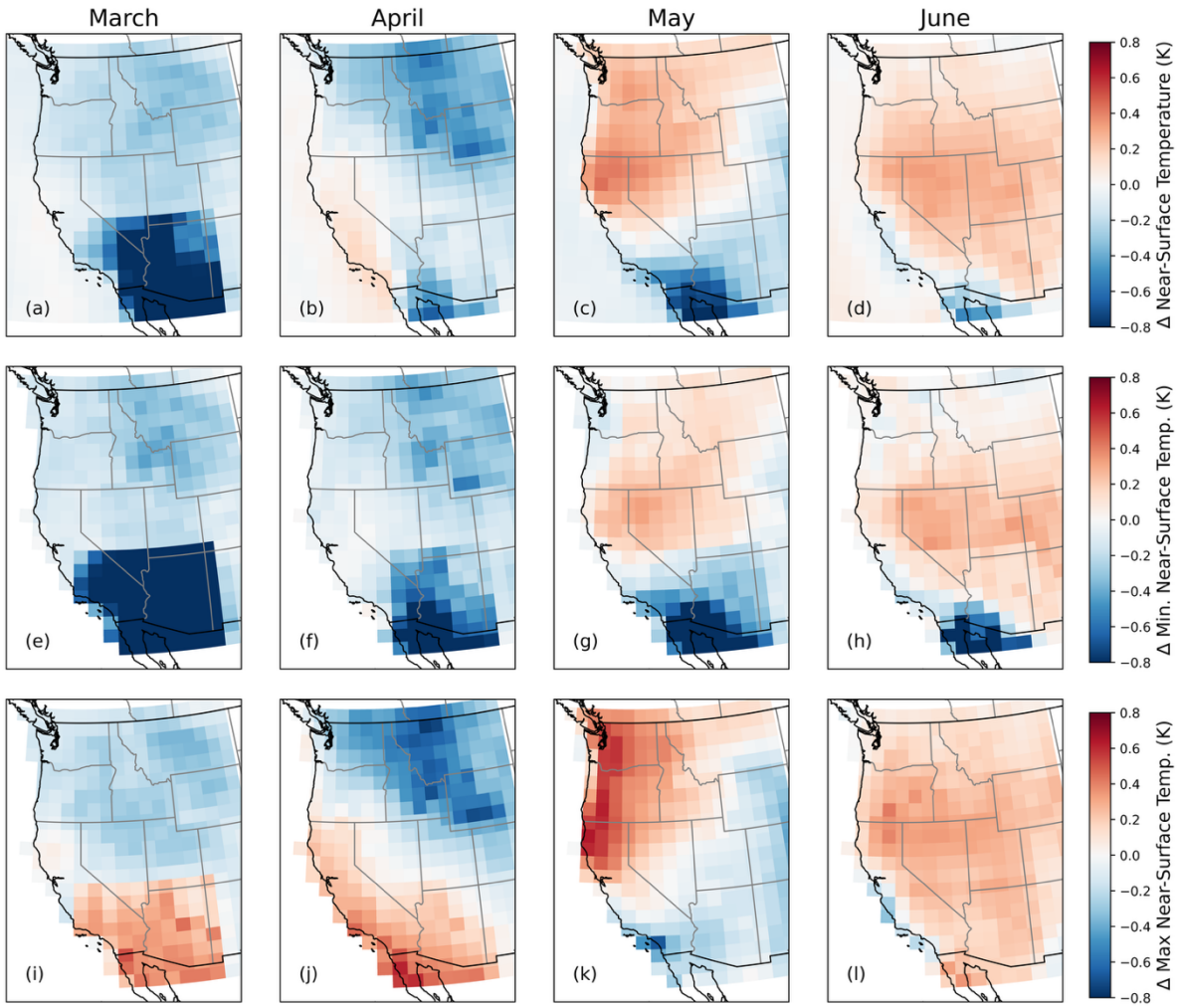

Fig. 3. March-June changes in (top) average (center) minimum and (bottom) maximum daily 2-m temperature as a result of March Southwest US soil moisture depletion, averaged across 108 ensemble members.

As a result of depleting surface soil moisture over the Southwest US at the start of March, we find warming in the Western US (WUS) across the average, minimum, and maximum daily near-surface temperature fields in May-June (right two columns in Fig. 3). The daily average temperature anomalies in May are roughly +0.3ºC over the Pacific Northwest while the daytime maximum temperature anomaly is as high as +0.6ºC over some grid cells. By June, warming becomes more widespread, extending over most of the WUS region and with an average temperature anomaly of +0.2ºC. The spatial pattern of warming in our experiments is consistent with observations of the WUS-STP, which also manifests most prominently over Southern Idaho and surrounding regions (cf. Fig. 1d with 3d). However,

unlike the WUS-STP, the warm anomalies fade in July and are entirely absent later in the summer (not shown).

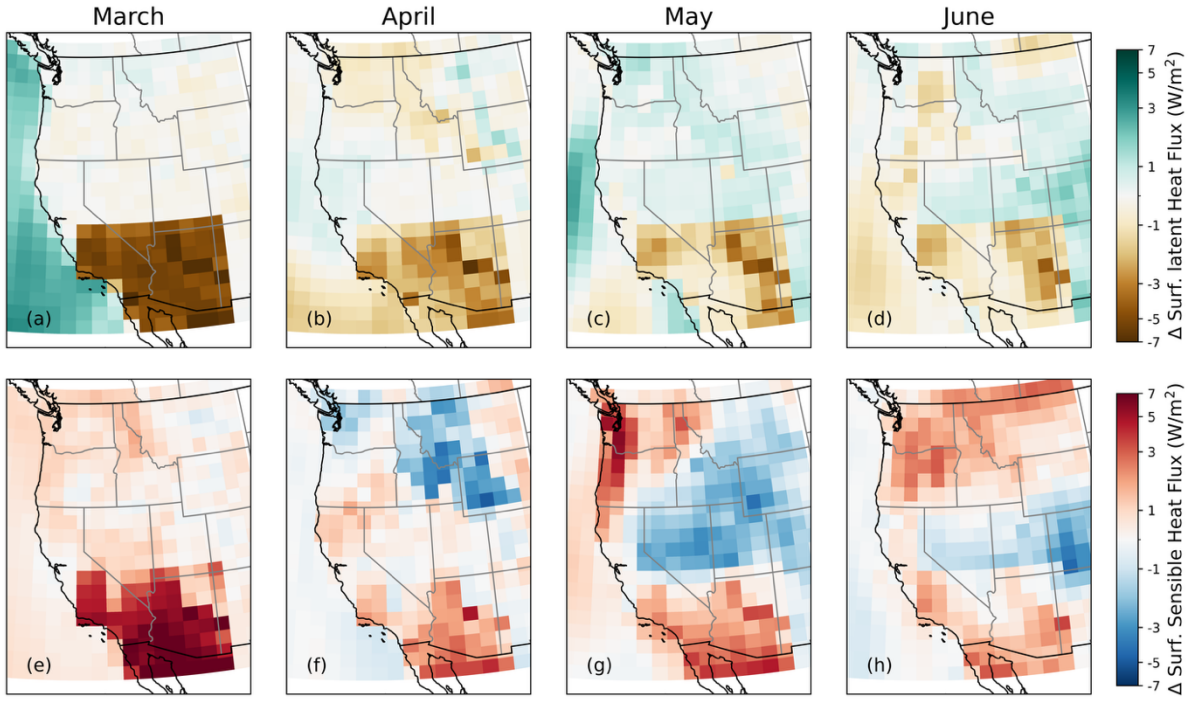

Fig. 4. March-June changes in surface (top) latent and (bottom) sensible heat flux (both positive upwards) as a result of March Southwest US soil moisture depletion, averaged across 108 ensemble members.

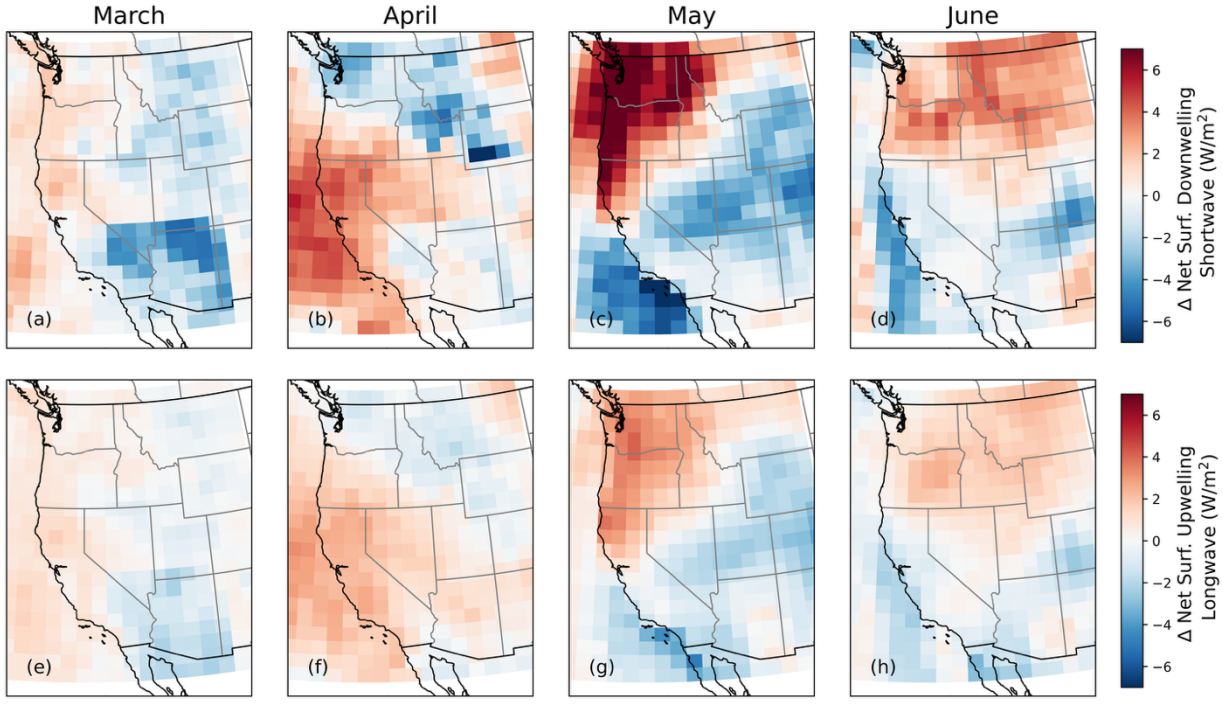

Fig. 5. As in Fig. 4, but for changes in net surface (top) shortwave and (bottom) longwave radiation (both positive downwards).

To explain the May-June temperature response, we analyze the relevant components of the surface energy budget (Figs. 4 and 5). Although early summer warming coincides with an increase in upward surface sensible heat flux over the Northwest US (Fig. 4g,h), there is only a weak accompanying decrease in upward latent heat flux that would link warming to changes in evaporative fraction (Fig. 4 c,d). Instead, we find a pronounced increase in net downwelling surface shortwave over the northern portion of our domain, particularly in May, that is spatially coincident with the temperature response (Fig. 5c, d; third columns of Fig. 4); this increase in solar heating is accompanied by a slightly weaker increase in surface upwelling longwave radiation that is consistent with the positive surface temperature anomaly. Over the central portion of our domain, we find the opposite to be true: solar heating and net upward surface longwave emission both decrease at the surface, which is consistent with the slight cooling in May (Fig. 3). The surface sensible heat flux also appears to decrease directly southeast of the warming, but this signature is interrupted by the lingering bounds of the soil moisture depletion patch imposed over the Southwest US (Fig. 4g).

Surprisingly, the daily average temperature decreases in March over the Southwest US by more than 0.8ºC where soil moisture was depleted (Fig. 3), despite sharp Bowen ratio changes in Figure 4 that would suggest the opposite (warming). We reconcile this finding by noting that the adiabatic cooling that is associated with the large-scale response in the second half of the month is greater than the daytime diabatic heating associated with the shift in the Bowen ratio due to soil moisture depletion (see Sect. 5). There is also a small cooling contribution from surface albedo in the first half of the month due to drier soils being brighter in nature and in our experiments (Ångström, 1925; Supplemental Figure S2). The cooling is thermodynamically balanced by a decrease in top of model outgoing longwave radiation (not shown).

4. Propagation of large-scale moisture anomalies

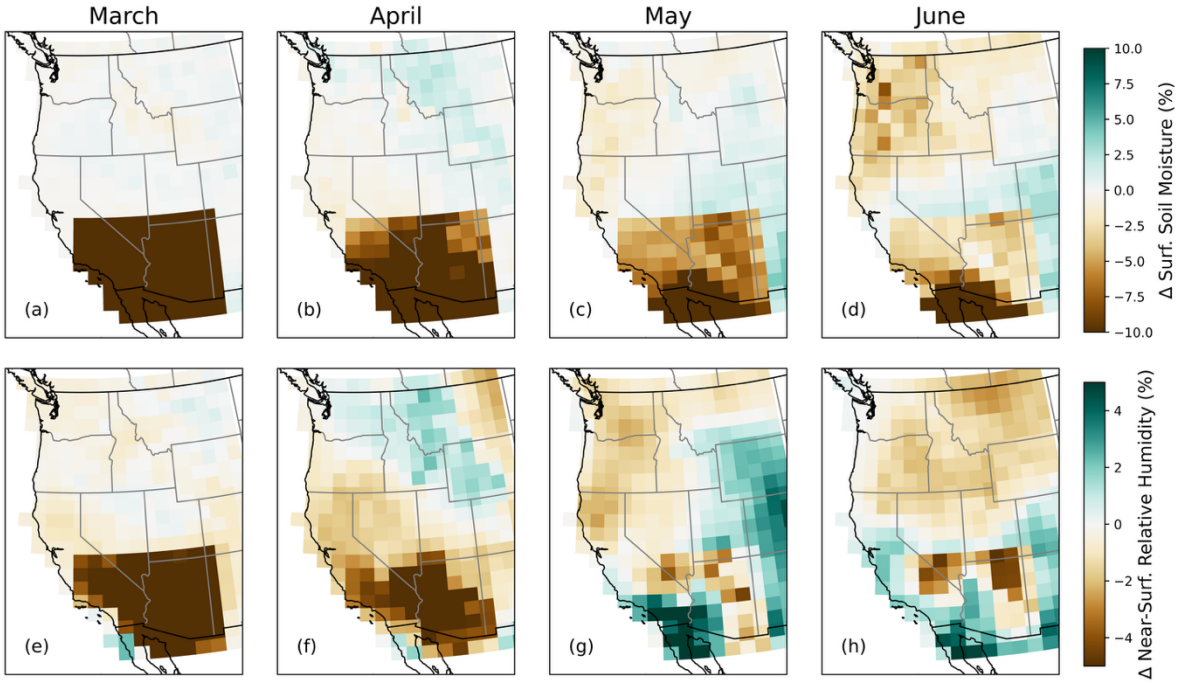

Fig. 6. March-June changes in (top) 10 CM soil moisture and (bottom) 2-m relative humidity as a result of March Southwest soil moisture depletion, averaged across 108 ensemble members. Both anomalies are computed as a percentage relative to monthly mean climatologies obtained from the control run.

Figure 6 shows the month-to-month evolution of surface soil moisture and low-level relative humidity anomalies in our experiments. Although we initially set soil moisture to zero at the start of March, soil moisture gradually increases over the Southwest US due to precipitation and snow melt (Fig. 6a-d). Across the six months of our experiment, the anomalies in surface soil moisture and low-level relative humidity appear to be correlated with one another (Fig. 6). From March to June, the surface soil moisture deficits initially have a strong impact on the overlying atmosphere and induce negative changes in low-level relative humidity over the Southwest that then appear to propagate northward to the Pacific Northwest by May. Unlike the temperature anomalies in our experiment, this pattern of soil moisture deficit persists well into July and August (not shown).

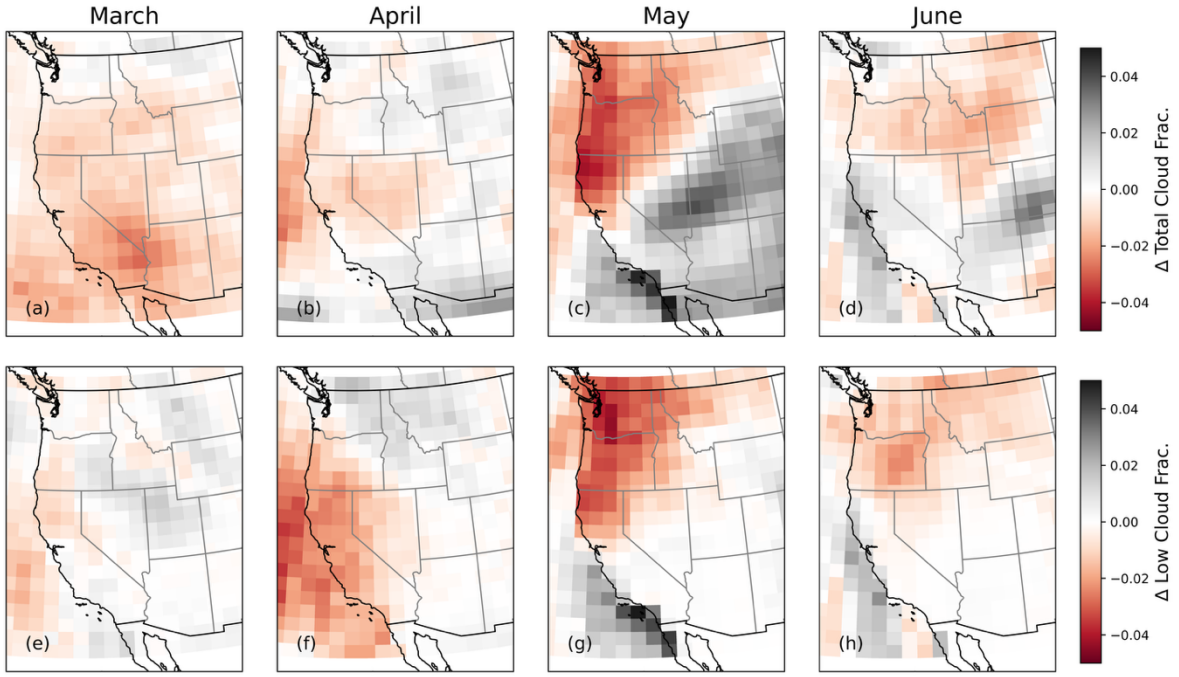

Fig. 7. Changes in (top) total cloud and (bottom) low cloud fraction as a result of March Southwest US soil moisture depletion, averaged across 108 ensemble members.

To understand the aforementioned changes in surface shortwave radiation that drive the May-June warming in our experiments, we note that decreases in low-level relative humidity (Figs. 6e-h) are accompanied by changes in cloudiness, particularly in the low cloud fraction (Figs. 7c,d,g,h). The albedo of low clouds is the primary contributor to the shortwave cloud radiative effect, and the decreases in low cloud fraction in May-June align with the areas of increased net downwelling shortwave in Figure 5c,d. These results confirm that changes in atmospheric moisture and cloudiness, not evaporative fraction, are what drive May-June warming in our experiment.

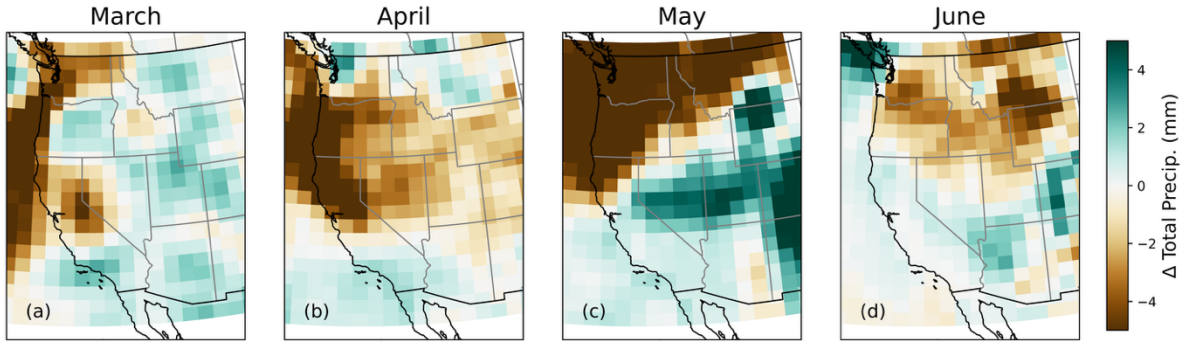

Fig. 8. Changes in total monthly precipitation as a result of March Southwest US soil moisture depletion, averaged across 108 ensemble members.

Total precipitation in the Northwest US also decreases in the experiment during April-June where there are coincident large-scale deficits in low-level relative humidity and

cloudiness (Fig. 8). The resulting pattern of precipitation anomalies in the northern domain in May-June is similar to the observed precipitation anomalies in summertime associated with springtime soil moisture deficits (cf. Fig. 8c, d with Fig. 1c). In May, positive precipitation anomalies appear over the Southwest and continue into June, which was also noted in observations (Fig. 1c). These increases in precipitation are accompanied by increases in cloud cover and, to some extent, relative humidity (despite a persisting surface soil moisture deficit). A recent study by Cleveland et al. (2025) found that early spring soil moisture deficits over the Colorado Plateau, which overlaps with our depletion region, are associated with an earlier North American Monsoon (NAM) onset and increased summertime precipitation over the Southwest US in reanalysis data. That we find similar relationships between early spring soil moisture anomalies and late spring atmospheric moisture over the Southwest US in our experiments is further evidence that the simulated teleconnection has some relevance to the real world.

The propagation of large-scale moisture anomalies from the Southwest US to Pacific Northwest from March to early summer in our experiments is strong evidence of teleconnection-like behavior which must be initiated by soil moisture variations, which raises the question: What drives changes in atmospheric circulation to provide a pathway for these soil moisture teleconnections?

5. Circumglobal circulation changes

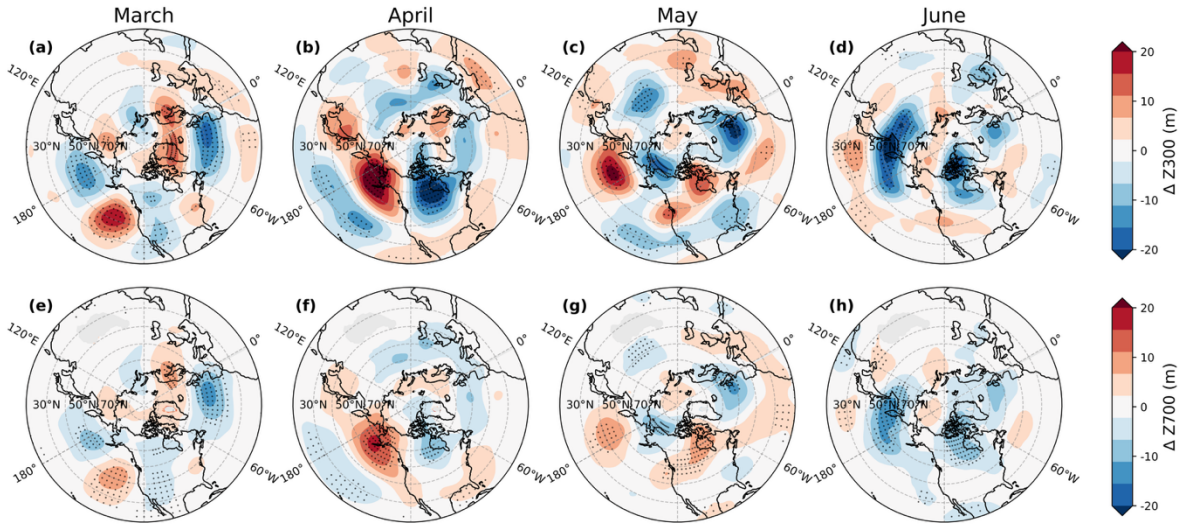

Fig. 9. March-June changes in (top) 300 and (bottom) 700 hPa geopotential heights as a result of March Southwest US soil moisture depletion, averaged across 108 ensemble members. Stippling indicates where the anomalies are significant at the 90% confidence level, based on a paired t-test.

To understand the large-scale response and connect March surface soil moisture deficit to subsequent changes in atmospheric moisture that appear in the Western US in April-June, we follow Koster et al. (2016) and Teng et al. (2019) and document the atmospheric circulation response to the soil moisture depletion. During spring, we find circumglobal changes that are vertically coherent throughout the troposphere (Fig. 9). Geopotential height anomalies in March and May form a nearly zonal pattern of alternating highs and lows in the midlatitudes that resembles a Rossby wave train. In March, a quasi-stationary high appears just off the West Coast of the US that deepens and extends north to form a meridional dipole stradling the west coast of North America in April. In May, a high-pressure anomaly over the Pacific Northwest coincides with large-scale warming and deficits in humidity, precipitation, and cloud fraction (Figs. 6g, 8c, and 6c), which persists into June but only aloft (Fig. 9d). The pattern of circulation anomalies in May-June (and the associated temperature and precipitation anomalies in Figs. 3cd, 8cd) strongly resemble the circulation responses to summertime moisture deficits previously demonstrated by Koster et al. (2016) and Teng et al. (2019) as well as observations of the summertime circulation anomalies associated with the WUS-STP (Vargas Zeppetello et al. 2024). As in their studies, decreased precipitation consistent with the upper-level positive height anomaly over the Northwest US drives near-surface drying and warming in May-June of our experiments. Earlier reductions in precipitation and cloudiness during April likely result from the blocking effect of the east-west dipole in height anomalies flanking the west coast of Canada and the reduction in the westerlies farther offshore along 45ºN, which acts to disrupt the supply of moisture from the Pacific to the California coast. This suggests that the drying of the soil moisture in May-June (Fig. 6) is forced by, rather than driving, the changes in precipitation and humidity aloft. From June onwards, the positive geopotential height anomalies weaken considerably and dissipate, along with the positive temperature anomalies, in late summer (not shown).

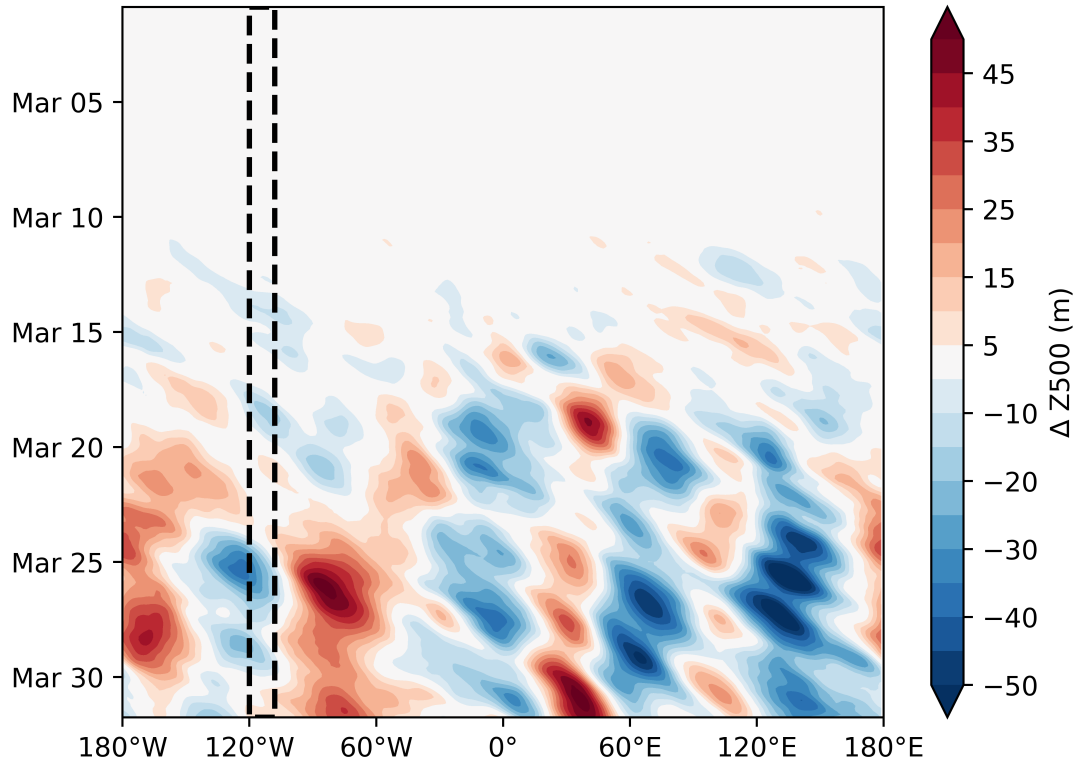

Fig. 10. Hovmöller diagram of March 3-hourly changes in Z500 following Southwest US (outlined) soil moisture depletion on March 1st, averaged from 40º-60ºN over 50 ensemble members.

Figure 10 presents the time evolution of the 500 mb geopotential height anomalies averaged between 40º-60ºN during the first month of the experiment as a Hovmöller diagram. Two weeks after the instantaneous depletion of surface soil moisture on March 1st, a nearly stationary wavenumber 4 Rossby wave sets in with a low center over the western US (~130ºW-90ºW); it takes a little over two weeks for the large-scale pattern to set up and become quasi-stationary, which is consistent with the two-week timescale Teng et al. (2019) found in their study.

Previous work by Branstator (1990, 2002) provides a framework for understanding how local heating sources can excite quasi-stationary wave anomalies within a linear barotropic vorticity model. Recent studies from Koster et al. (2016) and Teng et al. (2019) demonstrated that sensible heating over dry CONUS surfaces produces positive diabatic heating anomalies that are capable of instigating these circulation patterns. However, those studies focused on the contemporaneous circulation response to extended (i.e., 1-3 month) summertime soil moisture deficits prescribed over the Great Plains region and entire Western US domain. To explain the circulation response to a springtime soil moisture deficit in the Southwest US that

we find in our experiment, we examine the evolution of the overlying atmosphere during the first month of the experiment.

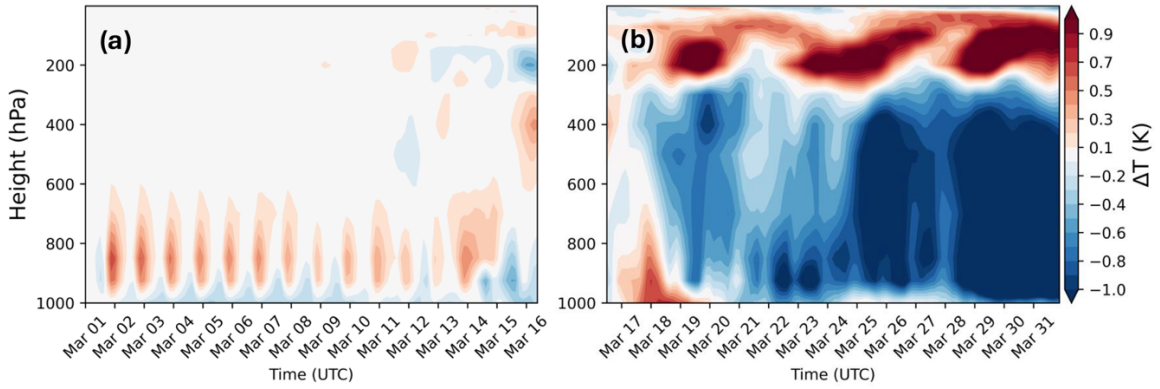

Fig. 11. Vertical changes in March 3-hrly temperature during (a) the first half and (b) the second half of the month following Southwest US soil moisture depletion on March 1st, averaged over the Southwest US depletion region for 50 ensemble members.

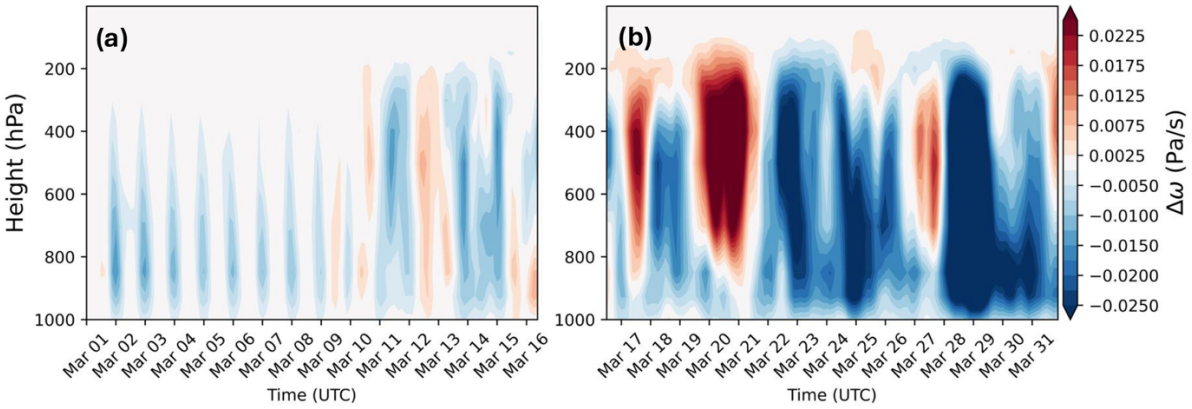

Fig. 12. Vertical changes in March 3-hrly vertical velocity (omega) in pressure coordinates during (a) the first half and (b) the second half of the month following Southwest US soil moisture depletion on March 1st, averaged over the Southwest US depletion region for 50 ensemble members.

Earlier in Section 3, we noted that the Southwest US experienced near-surface averaged cooling in the March monthly mean of our experiments (Fig. 3a). When we examine the composite time series of March air temperature anomalies averaged over the Southwest US, however, we find anomalously warm and rising air in the daytime that extends throughout the troposphere during the first half of the month (Figs. 11a, 12a, S3a, S4a). In the two weeks immediately following surface soil moisture depletion, temperatures warm by approximately 0.2-0.6ºC from the surface up to 600 hPa, with the strongest warming occurring near the surface during the daytime (Fig. 11a). The negative ω anomalies extend upwards to about 400 hPa (Fig 12a.). At around the two-week mark, the overlying atmosphere gradually becomes dominated by the deep, larger scale motions driven by the circulation response (c.f.

Fig. 10)—which, again, is consistent with the timescales displayed in previous studies. The negative temperature anomalies in the second half of the month (Fig. 11b, S3b, S3d) are associated with upward vertical motion ($\omega < 0$; Fig. 12b, S4b, S4d), which is indicative of adiabatic cooling of the troposphere over the Southwest US. The shift from localized heating in the first half of the month to large-scale cooling is summarized in Figure 13, which shows the vertical profile of daytime (Fig. 13a, b) and nighttime (Fig. 13c, d) temperatures over the Southwest US. We hypothesize that the stretching associated with daytime warming in the first half of the month provides a vorticity source that is responsible for the low that forms over the Southwest US (Fig. 9a, e; 10) in the second half of the month, and that the large-scale circumglobal circulation response is shaped by the climatological waveguide.

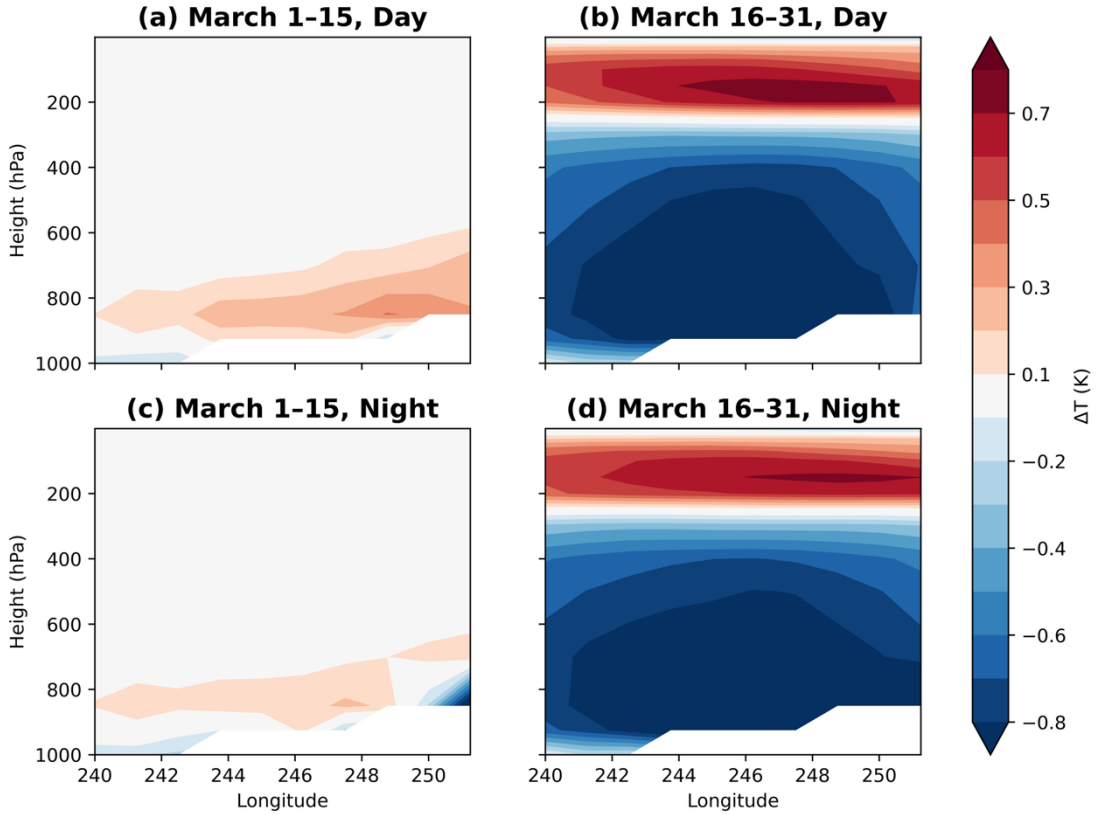

Figure 13. Vertical changes in early (left) and late (right) March daytime (top) and nighttime (bottom) vertical velocity (omega) as a result of March Southwest US soil moisture depletion, averaged across the latitudes of the depletion region (30-38ºN) over 50 ensemble members.

6. The amplitude of the simulated response compared to observations

The hypotheses motivating our study are primarily based upon our knowledge of the WUS-STP from observations (Vargas Zeppetello et al. 2024). While it is difficult to make direct comparisons between the results of our instantaneous forcing and the real-world MAM soil moisture deficits associated with the WUS-STP, we find strong evidence that the teleconnections and processes acting to produce early summer temperature anomalies in our experiment are also relevant to producing the pattern of observed summertime temperature anomalies in the Western US.

To evaluate the amplitude of the simulated response to a March soil moisture perturbation against observations, we first create an index of March soil moisture in the Southwest US by averaging detrended satellite measurements of soil moisture over the depletion region in our experiments (see Methods). Following Koster et al. (2016), we then standardize the soil moisture anomalies before regressing them upon observations of summertime temperature and circulation. Vargas Zeppetello et al. (2024) demonstrated that MAM soil moisture anomalies in the Western US are well-correlated throughout the soil column, down to a depth of 50 cm; in our depletion experiments, we find that climatological March 50 cm soil moisture is reduced by ~1.2σ on average over the Southwest US. To be consistent in our comparison between observed and simulated amplitudes, we scale the observed response to reflect a 1.2σ reduction in Southwest US March 50 cm soil moisture. In the following comparisons, we focus on assessing the simulated response in May-June since, unlike in the modeling experiments, it is not possible to extract the contemporaneous atmospheric circulation response to soil moisture anomalies in March from the atmospheric circulation that produced the soil moisture anomalies. We also focus on the maximum features of the observed and simulated responses; to compare their amplitudes, we average over the subset of the Western US domain where circulation anomalies are statistically significant in each dataset (Fig. 14).

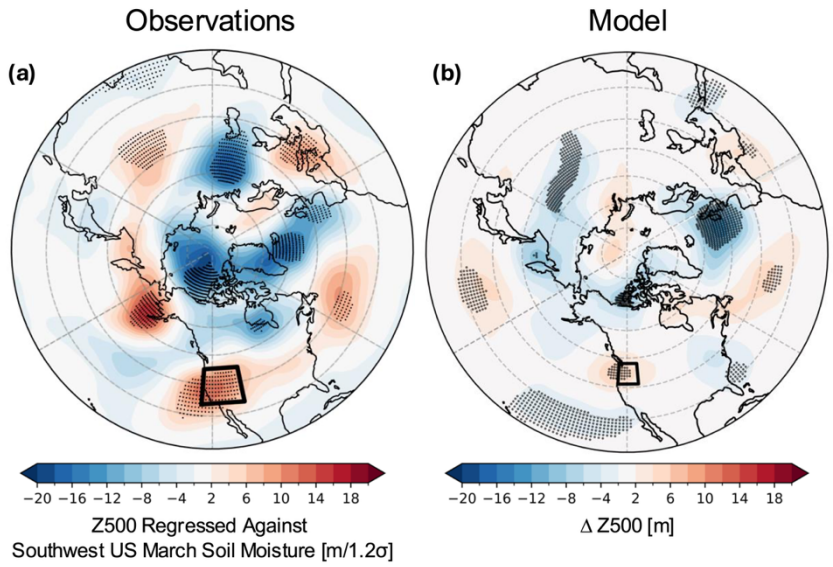

Fig. 14. (a) May-June 500 mb geopotential heights (Z500) from ERA5 regressed upon high pass-filtered March average soil moisture across the Southwest US depletion domain from ESA CCI. (b) The May-June Z500 change in our depleted soil moisture experiments. Stippling indicates where anomalies and regression coefficients are significant at the 90% confidence level. Anomalies in (a) are scaled to match the 1.2σ reduction in 50 cm Southwest US March soil moisture generated by our experiment.

When we regress May-June 500 mb heights (Z500) from ERA5 against our standardized soil moisture index, we observe (scaled) circulation anomalies that resemble, but are stronger than, the simulated response. In observations, a 1.2σ reduction in Southwest US March soil moisture is associated with an average May-June 500 mb geopotential height anomaly of +10.4 m over the Western US (Fig. 14a, outlined domain). In contrast, Z500 only increases by an average of 4.5 m over the Western US in May-June of our experiments (Fig. 14b, outlined domain). This suggests that the amplitude of the simulated circulation response may be too weak in the model—despite it reproducing the position of the WUS high pressure anomaly. Similarly, Koster et al. (2016) also reported that the circulation response to prescribed soil moisture anomalies was weaker in their model than in nature. Although we are primarily focused on the model's ability to reproduce the observed Western US pattern, we note that there are key similarities between the observed and simulated response elsewhere in our experiments—particularly over the North Atlantic (high) and Western Europe (low). Farther away from the source region, however, these similarities gradually disappear, as expected. The pattern correlation between the observed and simulated 500 mb geopotential height anomalies is r=0.40 between 40-60ºN in the Western Hemisphere and r=0.08 across all longitudes.

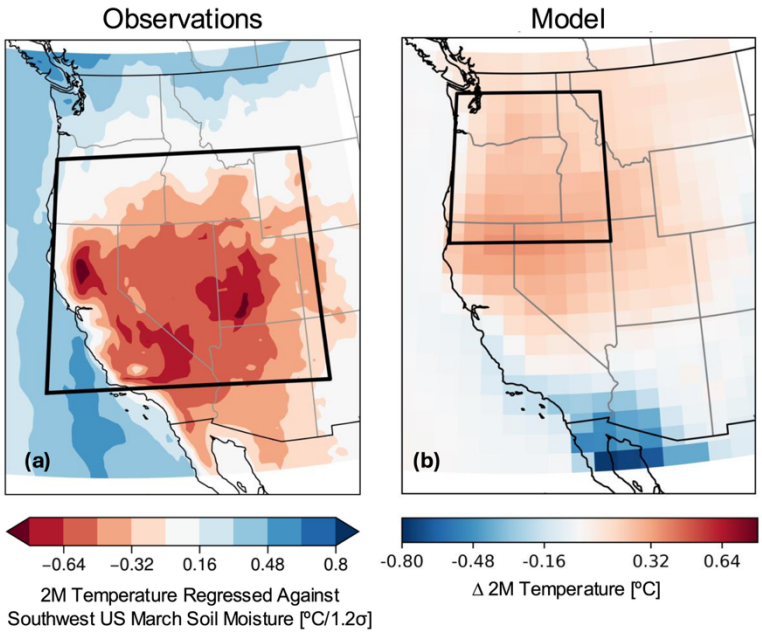

Fig. 15. (a) May-June 2-m air temperature from ERA5 regressed upon high pass-filtered March average soil moisture across the Southwest US depletion domain from ESA CCI. (b) The May-June 2-m air temperature change in our depleted soil moisture experiments. Anomalies in (a) are scaled to match the 1.2σ reduction in 50 cm Southwest US March soil moisture generated by our experiment.

Finally, we compare the amplitude of the simulated temperature response to observations by regressing May-June temperature from ERA5 upon the March soil moisture index. From Figure 15a, we expect May-June temperatures to warm by an average of 0.32ºC over the Western US (outlined) in response to a 1.2σ reduction in Southwest US March soil moisture in observations. Our experiments, however, only simulate ~66% of the observed temperature response (0.21ºC; Fig. 15b).

Given our hypothesis that circulation changes drive May-June warming in our experiments, that a weak circulation response would also lead to weak temperature anomalies is consistent with our understanding of the processes that modulate summertime temperature variability over the Western US. We note that the relationship between Western US summertime warming and springtime soil moisture anomalies in the five other CMIP6 models analyzed by Vargas Zeppetello et al. (2024) was also considerably weaker than in observations. While identifying model processes leading to this bias is beyond the scope of this paper, we hypothesize that the weak amplitudes of the circulation and temperature anomalies in early summer are related to the weaker persistence in the simulated response compared to that in observations.

7. The persistence of the simulated response

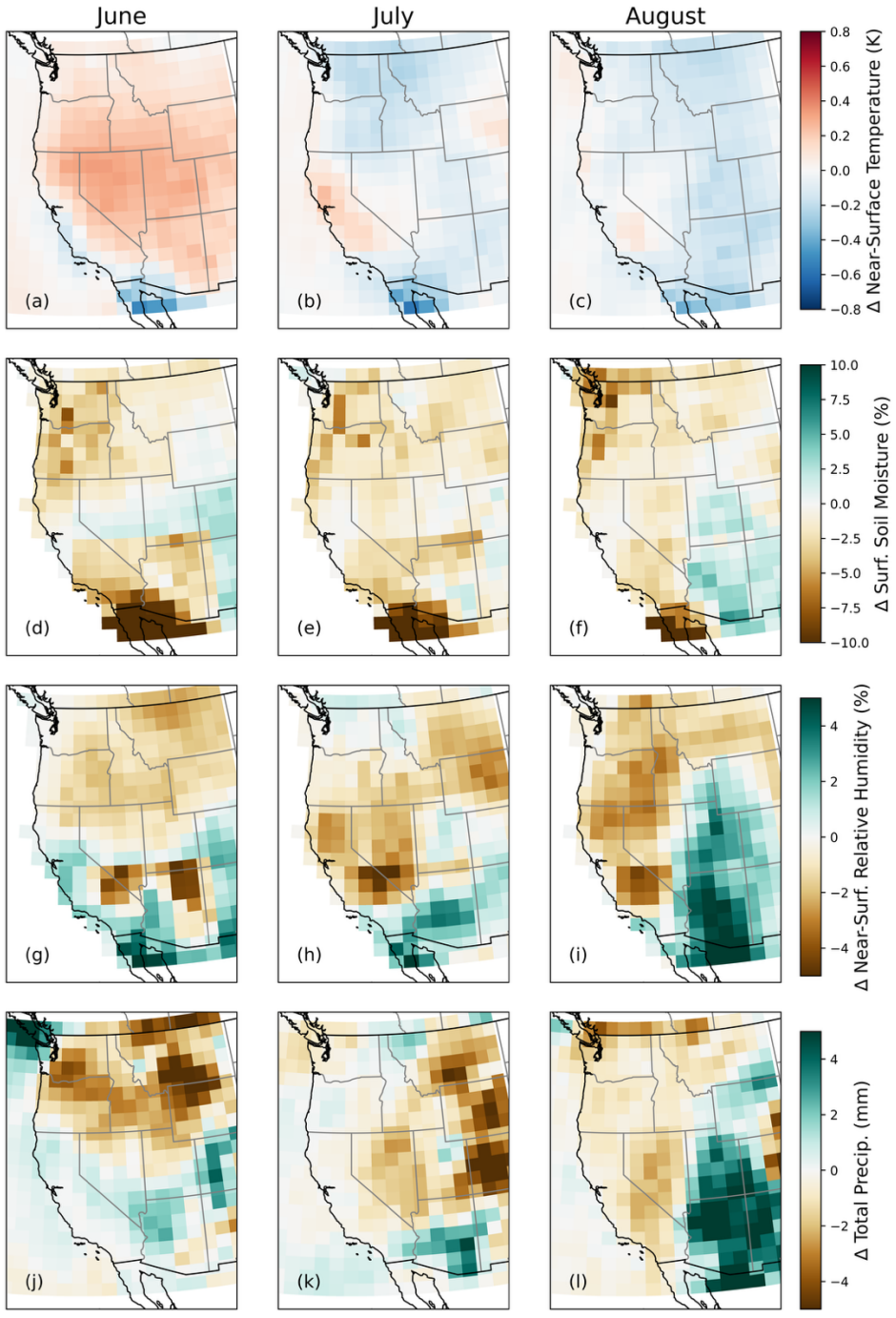

441

442 Figure 16. Changes in JJA (a-c) 2-meter temperature (d-f) 10 cm soil moisture (g-i) 2-meter relative
443 humidity (j-l) total monthly precipitation as a result of March Southwest US soil moisture depletion,
444 averaged across 108 ensemble members.

445 In the previous section, we hypothesized that an insufficiently large circulation response
446 would produce a weaker and, subsequently, less persistent simulated temperature response.
447 The weak temperature response in our experiments is consistent with the weaker relationships
448 between summertime JJA temperature and springtime MAM soil moisture variability

449 previously found in CESM2 (c.f., Figure 1b, 1f). Here, we present a few additional processes
450 that could influence and explain its persistence.

451 Koster et al. (2016) introduced a framework for understanding how feedbacks between
452 circulation anomalies (high pressure), surface meteorological anomalies (warming and
453 drying), and diabatic heating anomalies (sensible heating) act to enhance and sustain the
454 initial atmospheric response to soil moisture anomalies. To explain the discrepancy between
455 the magnitude of the simulated and observed responses in their study, they hypothesized that
456 these land-atmosphere feedbacks were too weak in the model they used. In our experiments,
457 we find that soil moisture anomalies in the Northwest US do persist into late summer unlike
458 the temperature response (Figure 16a-c, d-f). Furthermore, these soil moisture anomalies
459 drive changes in surface sensible (positive) and latent (negative) heat flux in an area that
460 aligns with the observed summertime temperature pattern (Figure 17a-f). This is strong
461 evidence that our model does simulate the correct teleconnection, but the feedbacks between
462 surface fluxes and circulation anomalies in late summer may be too weak in CESM2—
463 leading to a short-lived temperature anomaly.

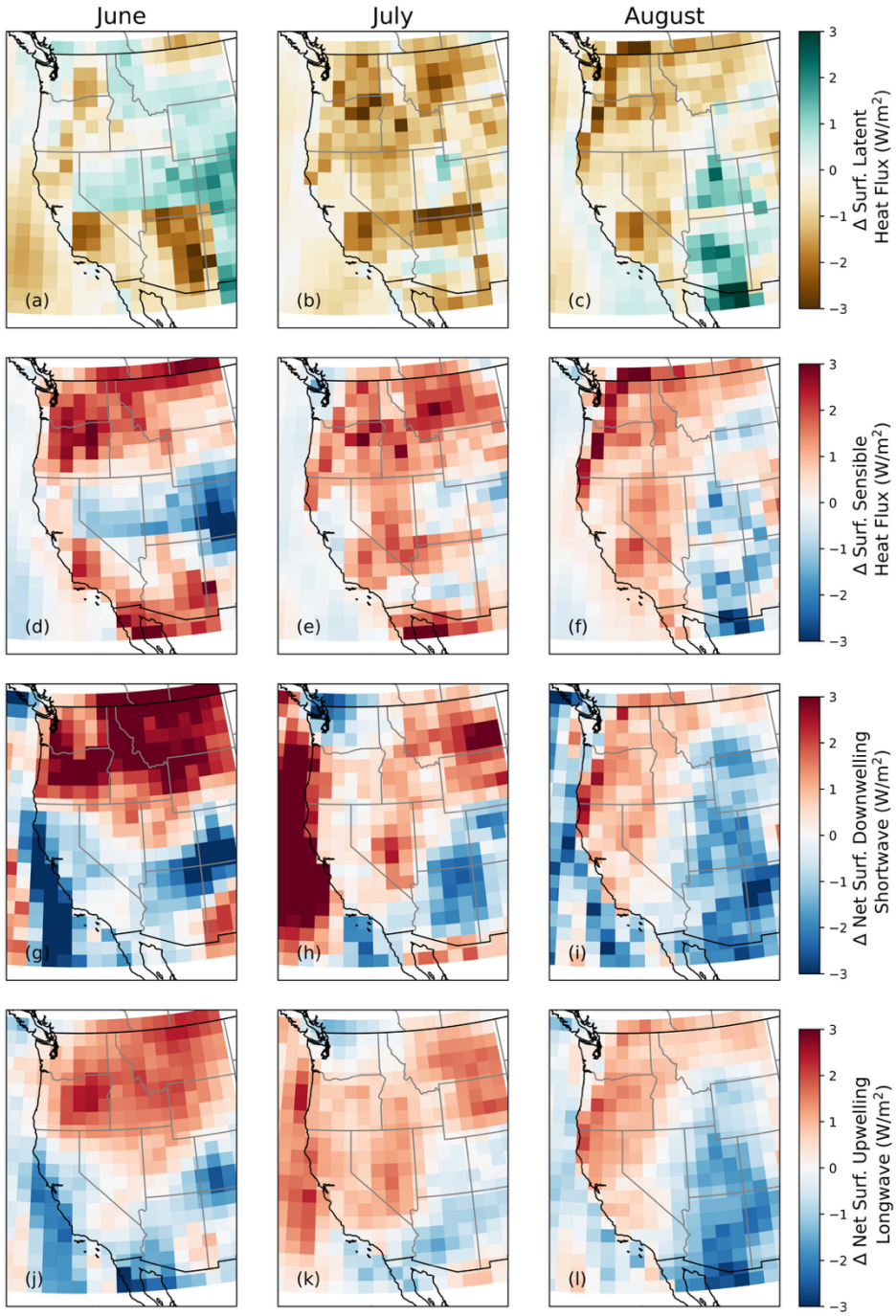

Figure 17. Changes in JJA surface (a-c) latent heat flux (d-f) sensible heat flux (g-i) net downwelling shortwave (j-l) net upwelling longwave as a result of March Southwest US soil moisture depletion, averaged across 108 ensemble members.

In addition to the aforementioned positive feedbacks, we also note that drying over the WUS-STP region is accompanied by an increase in net upward longwave radiation at the surface during July-August (Figure 17j-l). Decreases in surface evaporation decrease atmospheric water vapor, resulting in a weaker greenhouse effect that promotes greater longwave cooling to space (Laguë et al. 2021, 2023). This longwave cooling is a negative

feedback that offsets the increases in sensible heating from surface drying, also contributing to a weaker overall temperature response in our experiments.

Lastly, Vargas Zeppetello et al. (2024) found that the circulation anomalies associated with summertime warming in observations drive a weak SST response in the central North Pacific. Hence, prescribing climatological SST in our experiments amounts to a dampening of the circulation anomalies that may have otherwise persisted into late summer. Future work may want to consider conducting these experiments in a model with coupled SSTs.

8. Conclusion

In this study, we explored the potential for regional springtime soil moisture variations to produce distal teleconnections in summertime temperature and precipitation through land-atmosphere interactions. Building from observations that connect anomalously warm and dry conditions in summer in the Western US to deficits in springtime soil moisture in the Southwest US, we performed an ensemble of experiments using the CESM2 and set the near-surface soil moisture in the Southwest US to zero on March 1st each year. As a result, we found:

I. In March: Reductions in surface latent heat flux over the Southwest US persist to drive daytime diabatic heating anomalies that extend into the upper troposphere during the first half of the month, exciting a large-scale (circumglobal) quasi-stationary wave response.

II. From late March-May: The circumglobal circulation response gives rise to large-scale deficits in precipitation, near-surface relative humidity, and cloudiness over the Western United States.

III. In May-June: Decreases in low-cloud fraction promote widespread warming that begins in the Pacific Northwest through the shortwave cloud radiative effect. Warming is accompanied by Northwest US surface soil moisture deficits that persist into late summer.

In summary, we have demonstrated a new pathway for springtime soil moisture anomalies to have a non-local impact on summertime climate in the Western US. Our results are generally consistent with the observed relationships between springtime soil moisture variations in the Southwest US and summertime temperature and circulation anomalies across the Western US (Vargas Zeppetello et al., 2024). However, the amplitudes of the

simulated temperature and circulation responses in early summer are weaker than observed variations associated with a comparable reduction in Southwest US MAM soil moisture, which may also negatively impact persistence. To explain this behavior, we showed how model biases, fixed SSTs, and negative feedbacks could all contribute to the diminished temperature and circulation response in July-August of our experiments.

Though the results of our experiments demonstrate that soil moisture deficits over the Southwest US in March *cause* May-June warming across the Western US, there are a few aspects of the proposed pathway that merit further investigation. First, we would like to investigate the relationship between the amplitude and persistence of the summertime temperature and circulation anomalies to the depth, magnitude, and sign of the initial soil moisture anomaly imposed in springtime. Results from sensitivity studies performed by Teng et al. (2019) whereby soil moisture anomalies of various amplitudes and depths were imposed throughout the summer suggest that the pattern of circulation anomalies simulated in our experiments will be relatively insensitive to these details, but that the amplitude of the response would scale linearly with the strength of the soil moisture anomaly. Second, we would like to perform wave activity and vorticity budget analyses to better understand how the atmospheric circulation anomalies develop in March and continue to evolve in April in response to March soil moisture deficits to produce the pattern of highs and lows in May. Finally, we would like to test whether other climate models reproduce our results in CESM2. Given that the five other CMIP6 models analyzed by Vargas Zeppetello et al. (2024) displayed similar relationships between springtime soil moisture and summertime temperature in their free-running simulations, there is reason to expect consistent representation of the WUS-STP and the physical processes that drive it across climate models.

The presence of soil moisture teleconnections in the Western US extends our understanding of the spatial and temporal scales of land-atmosphere interactions. Our finding that springtime soil moisture deficit in the Southwest US leads to summertime warming and drying across the Western US can potentially be used to improve seasonal forecasts for the region and, more broadly, highlights the need for accurate land initialization schemes within operational models. Moving forward, we are interested in using our methodology to identify similar, teleconnection-like patterns in other regions where antecedent soil moisture conditions may have non-local impacts on climate.

Acknowledgments.

The authors thank Abby Swann and Cecilia Bitz for providing their CESM2 expertise and other scientific insights. LNZ is supported by the National Science Foundation Graduate Research Fellowship under Grant No. DGE-2140004. DSB was supported by a grant from the Tamaki Foundation. High-performance computing support from the Derecho system (doi:10.5065/qx9a-pg09) was provided by the NSF National Center for Atmospheric Research (NCAR), sponsored by the National Science Foundation.

Data Availability Statement.

All observational datasets used in this study are publicly available. The numerical model simulations upon which this study is based are too large to archive. Instead, we provide detailed instructions for replicating the simulations in Section 2, Methods. The model version used was CESM2.1.5.

REFERENCES

Ångström, A., 1925: The Albedo of Various Surfaces of Ground. *Geogr. Ann.*, **7**, 323–342, https://doi.org/10.1080/20014422.1925.11881121.

——, 1935: Teleconnections of Climatic Changes in Present Time. *Geogr. Ann.*, **17**, 242–258, https://doi.org/10.2307/519964.

Berg, A., B. Lintner, K. Findell, and A. Giannini, 2017: Soil Moisture Influence on Seasonality and Large-Scale Circulation in Simulations of the West African Monsoon. *J. Clim.*, **30**, 2295–2317, https://doi.org/10.1175/JCLI-D-15-0877.1.

Branstator, G., 1990: Low-Frequency Patterns Induced by Stationary Waves. *J. Atmospheric Sci.*, **47**, 629–648, https://doi.org/10.1175/1520-0469(1990)047%3C0629:LFPIBS%3E2.0.CO;2.

——, 2002: Circumglobal Teleconnections, the Jet Stream Waveguide, and the North Atlantic Oscillation. *J. Clim.*, **15**, 1893–1910, https://doi.org/10.1175/1520-0442(2002)015%3C1893:CTTJSW%3E2.0.CO;2.

Cleveland, Z., M. Laguë, and C. Strong, 2025: North American Monsoon Response to Antecedent Soil Moisture and Snow in the Colorado Plateau. *J. Geophys. Res. Atmospheres*, **130**, e2024JD043026, https://doi.org/10.1029/2024JD043026.

568 Danabasoglu, G., and Coauthors, 2020: The Community Earth System Model Version 2
569 (CESM2). *J. Adv. Model. Earth Syst.*, **12**, e2019MS001916,
570 https://doi.org/10.1029/2019MS001916.

571 Delworth, T., and S. Manabe, 1989: The Influence of Soil Wetness on Near-Surface
572 Atmospheric Variability. *J. Clim.*, **2**, 1447–1462, https://doi.org/10.1175/1520-
573 0442(1989)002%3C1447:TIOSWO%3E2.0.CO;2.

574 Dingman, S. L., 2002: *Physical Hydrology*. Second Edition. Prentice Hall.

575 Dirmeyer, P. A., 2000: Using a Global Soil Wetness Dataset to Improve Seasonal Climate
576 Simulation. *J. Clim.*, **13**, 2900–2922, https://doi.org/10.1175/1520-
577 0442(2000)013%253C2900:UAGSWD%253E2.0.CO;2.

578 Dorigo, W., and Coauthors, 2017: ESA CCI Soil Moisture for improved Earth system
579 understanding: State-of-the art and future directions. *Remote Sens. Environ.*, **203**,
580 185–215, https://doi.org/10.1016/j.rse.2017.07.001.

581 ——, and Coauthors, 2021: The International Soil Moisture Network: serving Earth system
582 science for over a decade. *Hydrol. Earth Syst. Sci.*, **25**, 5749–5804,
583 https://doi.org/10.5194/hess-25-5749-2021.

584 Douville, H., 2002: Influence of Soil Moisture on the Asian and African Monsoons. Part II:
585 Interannual Variability. **15**, 701–720, https://doi.org/10.1175/1520-
586 0442(2002)015%3C0701:IOSMOT%3E2.0.CO;2.

587 Fennessy, M. J., and J. Shukla, 1999: Impact of Initial Soil Wetness on Seasonal Atmospheric
588 Prediction. **12**, 3167–3180, https://doi.org/10.1175/1520-
589 0442(1999)012%3C3167:IOISWO%3E2.0.CO;2.

590 Fischer, E. M., S. I. Seneviratne, P. L. Vidale, D. Lüthi, and C. Schär, 2007: Soil Moisture–
591 Atmosphere Interactions during the 2003 European Summer Heat Wave,
592 https://doi.org/10.1175/JCLI4288.1.

593 Guo, Z., P. A. Dirmeyer, and T. DelSole, 2011: Land surface impacts on subseasonal and
594 seasonal predictability. *Geophys. Res. Lett.*, **38**,
595 https://doi.org/10.1029/2011GL049945.

596 Harris, I., T. J. Osborn, P. Jones, and D. Lister, 2020: Version 4 of the CRU TS monthly
597 high-resolution gridded multivariate climate dataset. *Sci. Data*, **7**, 109,
598 https://doi.org/10.1038/s41597-020-0453-3.

599 Hersbach, H., B. Bell, P. Berrisford, A. Horányi, and and Coauthors,: ERA5 monthly
600 averaged data on single levels from 1940 to present, accessed 17 July 2025,
601 https://doi.org/10.24381/cds.f17050d7.

602 Koster, R. D., and Coauthors, 2010: Contribution of land surface initialization to subseasonal
603 forecast skill: First results from a multi-model experiment. *Geophys. Res. Lett.*, **37**,
604 https://doi.org/10.1029/2009GL041677.

605 ——, and Coauthors, 2011: The Second Phase of the Global Land–Atmosphere Coupling
606 Experiment: Soil Moisture Contributions to Subseasonal Forecast Skill. *J.*
607 *Hydrometeorol.*, **12**, 805–822, https://doi.org/10.1175/2011JHM1365.1.

608 Koster, R. D., Y. Chang, H. Wang, and S. D. Schubert, 2016: Impacts of Local Soil Moisture
609 Anomalies on the Atmospheric Circulation and on Remote Surface Meteorological
610 Fields during Boreal Summer: A Comprehensive Analysis over North America. *J.*
611 *Clim.*, **29**, 7345–7364, https://doi.org/10.1175/JCLI-D-16-0192.1.

612 Laguë, M. M., M. Pietschnig, S. Ragen, T. A. Smith, and D. S. Battisti, 2021: Terrestrial
613 Evaporation and Global Climate: Lessons from Northland, a Planet with a
614 Hemispheric Continent. *J. Clim.*, **34**, 2253–2276, https://doi.org/10.1175/JCLI-D-20-
615 0452.1.

616 Laguë, M. M., G. R. Quetin, and W. R. Boos, 2023: Reduced terrestrial evaporation increases
617 atmospheric water vapor by generating cloud feedbacks. *Environ. Res. Lett.*, **18**,
618 074021, https://doi.org/10.1088/1748-9326/acdbe1.

619 Lawrence, D. M., and A. G. Slater, 2008: Incorporating organic soil into a global climate
620 model. *Clim. Dyn.*, **30**, 145–160, https://doi.org/10.1007/s00382-007-0278-1.

621 ——, and Coauthors, 2019: The Community Land Model Version 5: Description of New
622 Features, Benchmarking, and Impact of Forcing Uncertainty. *J. Adv. Model. Earth*
623 *Syst.*, **11**, 4245–4287, https://doi.org/10.1029/2018MS001583.

624 Liu, D., G. Wang, R. Mei, Z. Yu, and M. Yu, 2014: Impact of initial soil moisture anomalies
625 on climate mean and extremes over Asia. *J. Geophys. Res. Atmospheres*, **119**, 529–
626 545, https://doi.org/10.1002/2013JD020890.

627 Liu, T., and Coauthors, 2023: Teleconnections among tipping elements in the Earth system.
628 *Nat. Clim. Change*, **13**, 67–74, https://doi.org/10.1038/s41558-022-01558-4.

629 Lorenz, R., E. B. Jaeger, and S. I. Seneviratne, 2010: Persistence of heat waves and its link to
630 soil moisture memory. *Geophys. Res. Lett.*, **37**,
631 https://doi.org/10.1029/2010GL042764.

632 McColl, K. A., S. H. Alemohammad, R. Akbar, A. G. Konings, S. Yueh, and D. Entekhabi,
633 2017: The global distribution and dynamics of surface soil moisture. *Nat. Geosci.*, **10**,
634 100–104, https://doi.org/10.1038/ngeo2868.

635 Muller, R. A., and Coauthors, 2014: A New Estimate of the Average Earth Surface Land
636 Temperature Spanning 1753 to 2011. *Geoinformatics Geostat. Overv.*, **2013**,
637 https://doi.org/10.4172/2327-4581.1000101.

638 Namias, J., 1991: Spring and Summer 1988 Drought over the Contiguous United States—
639 Causes and Prediction. *J. Clim.*, **4**, 54–65, https://doi.org/10.1175/1520-
640 0442(1991)004%3C0054:SASDOT%3E2.0.CO;2.

641 Pal, J. S., and E. A. B. Eltahir, 2001: Pathways Relating Soil Moisture Conditions to Future
642 Summer Rainfall within a Model of the Land–Atmosphere System.

643 Paolino, D. A., J. L. Kinter, B. P. Kirtman, D. Min, and D. M. Straus, 2012: The Impact of
644 Land Surface and Atmospheric Initialization on Seasonal Forecasts with CCSM. *J.*
645 *Clim.*, **25**, 1007–1021, https://doi.org/10.1175/2011JCLI3934.1.

646 Pincus, R., P. A. Hubanks, S. Platnick, K. Meyer, R. E. Holz, D. Botambekov, and C. J. Wall,
647 2023: Updated observations of clouds by MODIS for global model assessment. *Earth*
648 *Syst. Sci. Data*, **15**, 2483–2497, https://doi.org/10.5194/essd-15-2483-2023.

649 Rahmati, M., and Coauthors, 2024: Soil Moisture Memory: State-Of-The-Art and the Way
650 Forward. *Rev. Geophys.*, **62**, e2023RG000828,
651 https://doi.org/10.1029/2023RG000828.

652 Rai, A., S. K. Saha, S. Pokhrel, K. Sujith, and S. Halder, 2015: Influence of preonset land
653 atmospheric conditions on the Indian summer monsoon rainfall variability. *J.*
654 *Geophys. Res. Atmospheres*, **120**, 4551–4563, https://doi.org/10.1002/2015JD023159.

655 Rind, D., 1982: The Influence of Ground Moisture Conditions in North America on Summer
656 Climate as Modeled in the GISS GCM. *Mon. Weather Rev.*, **110**, 1487–1494,
657 https://doi.org/10.1175/1520-0493(1982)110%253C1487:TIOGMC%253E2.0.CO;2.

658 Ropelewski, C. F., and M. S. Halpert, 1987: Global and Regional Scale Precipitation Patterns
659 Associated with the El Niño/Southern Oscillation. *Mon. Weather Rev.*, **115**, 1606–
660 1626, https://doi.org/10.1175/1520-0493(1987)115%3C1606:GARSPP%3E2.0.CO;2.

661 Schär, C., D. Lüthi, U. Beyerle, and E. Heise, 1999: The Soil–Precipitation Feedback: A
662 Process Study with a Regional Climate Model. *J. Clim.*, **12**, 722–741,
663 https://doi.org/10.1175/1520-0442(1999)012%3C0722:TSPFAP%3E2.0.CO;2.

664 Seneviratne, S. I., T. Corti, E. L. Davin, M. Hirschi, E. B. Jaeger, I. Lehner, B. Orlowsky, and
665 A. J. Teuling, 2010: Investigating soil moisture–climate interactions in a changing
666 climate: A review. *Earth-Sci. Rev.*, **99**, 125–161,
667 https://doi.org/10.1016/j.earscirev.2010.02.004.

668 Shukla, J., and Y. Mintz, 1982: Influence of Land-Surface Evapotranspiration on the Earth's
669 Climate. *Science*, **215**, 1498–1501, https://doi.org/10.1126/science.215.4539.1498.

670 Small, E. E., 2001: The influence of soil moisture anomalies on variability of the North
671 American Monsoon System. *Geophys. Res. Lett.*, **28**, 139–142,
672 https://doi.org/10.1029/2000GL011652.

673 Teng, H., G. Branstator, A. B. Tawfik, and P. Callaghan, 2019: Circumglobal Response to
674 Prescribed Soil Moisture over North America. *J. Clim.*, **32**, 4525–4545,
675 https://doi.org/10.1175/JCLI-D-18-0823.1.

676 Trenberth, K. E., G. W. Branstator, D. Karoly, A. Kumar, N.-C. Lau, and C. Ropelewski,
677 1998: Progress during TOGA in understanding and modeling global teleconnections
678 associated with tropical sea surface temperatures. *J. Geophys. Res. Oceans*, **103**,
679 14291–14324, https://doi.org/10.1029/97JC01444.

680 Ullah, W., W. Guojie, Z. Gao, D. F. T. Hagan, A. S. Bhatti, and C. Zhua, 2021: Observed
681 Linkage between Tibetan Plateau Soil Moisture and South Asian Summer

682 Precipitation and the Possible Mechanism. *J. Clim.*, **34**, 361–377,
683 https://doi.org/10.1175/JCLI-D-20-0347.1.

684 Vargas Zeppetello, L. R., D. S. Battisti, and M. B. Baker, 2022: The Physics of Heat Waves:
685 What Causes Extremely High Summertime Temperatures? *J. Clim.*, **35**, 2231–2251,
686 https://doi.org/10.1175/JCLI-D-21-0236.1.

687 ——, L. N. Zhang, D. S. Battisti, and M. M. Laguë, 2024: How Much Does Land–
688 Atmosphere Coupling Influence Summertime Temperature Variability in the Western
689 United States? *J. Clim.*, **37**, 3457–3478, https://doi.org/10.1175/JCLI-D-23-0716.1.

690 Walker, G. T., and E. W. Bliss, 1932: World Weather V. *Mem. R. Meteorol. Soc.*, **4**, 53–84.

691 Wu, W., and R. E. Dickinson, 2004: Time Scales of Layered Soil Moisture Memory in the
692 Context ofLand–Atmosphere Interaction. *J. Clim.*, **17**, 2752–2764,
693 https://doi.org/10.1175/1520-0442(2004)017%3C2752:TSOLSM%3E2.0.CO;2.

694 ——, ——, H. Wang, Y. Liu, and M. Shaikh, 2007: Covariabilities of spring soil moisture
695 and summertime United States precipitation in a climate simulation. *Int. J. Climatol.*,
696 **27**, 429–438, https://doi.org/10.1002/joc.1419.

697 Xue, Y., and Coauthors, 2022: Spring Land Temperature in Tibetan Plateau and Global-Scale
698 Summer Precipitation: Initialization and Improved Prediction. *Bull. Am. Meteorol.*
699 *Soc.*, **103**, E2756–E2767, https://doi.org/10.1175/BAMS-D-21-0270.1.

700 Zhou, S., and Coauthors, 2019: Land–atmosphere feedbacks exacerbate concurrent soil
701 drought and atmospheric aridity. *Proc. Natl. Acad. Sci.*, **116**, 18848–18853,
702 https://doi.org/10.1073/pnas.1904955116.

703

704

Supplemental Figures

Figure S1: Timeseries of MAM soil moisture in the upper 9 cm of soil in our experiments (orange), control run (blue), and observations (black).

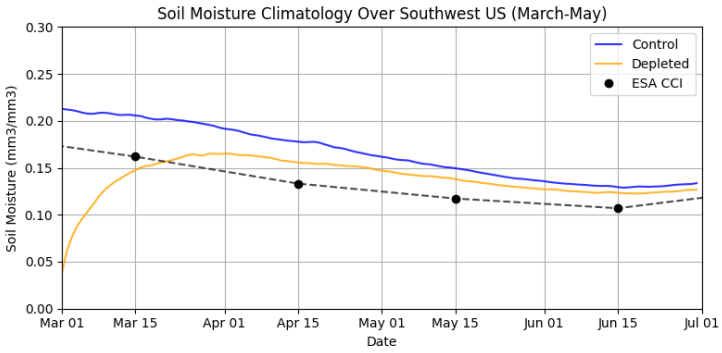

Figure S2: Changes in surface albedo as a result of March Southwest US soil moisture depletion, averaged across 108 ensemble members.

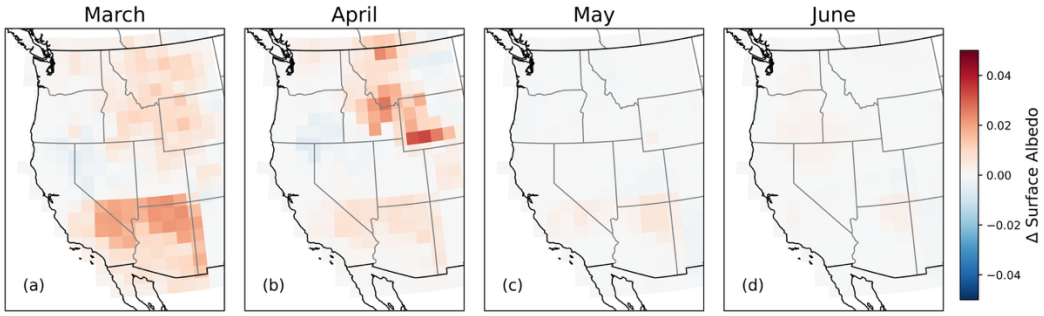

Figure S3: Early (left) and late (right) March changes in daytime (top) and nighttime (bottom) 2-m temperature as a result of March Southwest US soil moisture depletion, averaged across 50 ensemble members.

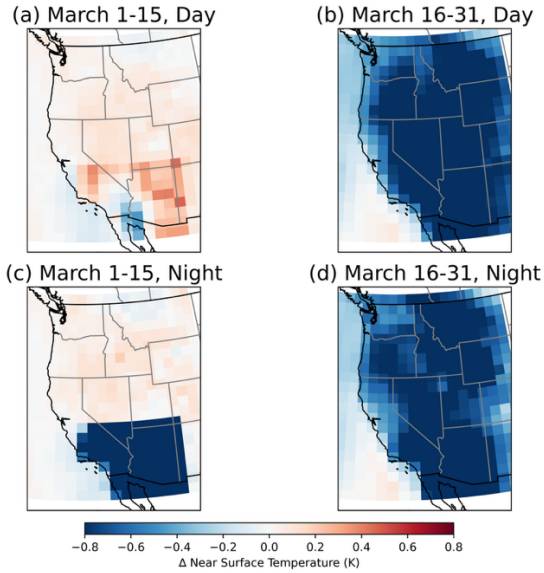

Figure S4: Vertical changes in early (left) and late (right) March daytime (top) and nighttime (bottom) vertical velocity (omega) as a result of March Southwest US soil moisture depletion, averaged across the latitudes of the depletion region (30-38ºN) over 50 ensemble members.

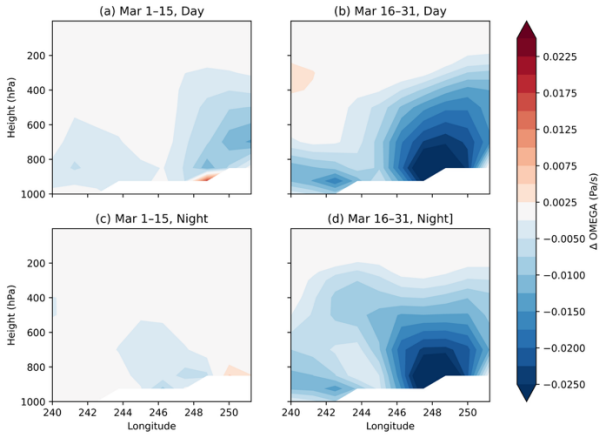

Figure S5: (a) May-June cloud fraction from MODIS COSP (Pincus et al. 2023) regressed upon high pass-filtered March average soil moisture across the Southwest US depletion domain from ESA CCI. (b) The May-June change in cloud cover in our depleted soil moisture experiments. Anomalies in (a) are scaled to match the 1.2σ reduction in 50 cm Southwest US March soil moisture generated by our experiment.